

# Geophysical Research Letters®

## RESEARCH LETTER

10.1029/2022GL099994

### Key Points:

- The Electron Losses and Fields Investigations observations of electromagnetic ion cyclotron-driven precipitation of relativistic electrons
- Test-particle model reproduce precipitating electron energy range
- Electron precipitation is caused by interplay of nonlinear resonant effects and the diffusive scattering

### Supporting Information:

Supporting Information may be found in the online version of this article.

### Correspondence to:

V. S. Grach,  
vsgrach@ipfran.ru

### Citation:

Grach, V. S., Artemyev, A. V., Demekhov, A. G., Zhang, X.-J., Bortnik, J., Angelopoulos, V., et al. (2022). Relativistic electron precipitation by EMIC waves: Importance of nonlinear resonant effects. *Geophysical Research Letters*, 49, e2022GL099994. <https://doi.org/10.1029/2022GL099994>

Received 12 JUN 2022

Accepted 25 AUG 2022

### Author Contributions:

**Conceptualization:** Anton V. Artemyev, Andrei G. Demekhov, Jacob Bortnik, Vassilis Angelopoulos

**Data curation:** Ethan Tsai, Colin Wilkins, Owen W. Roberts

**Formal analysis:** Veronika S. Grach, Anton V. Artemyev, Xiao-Jia Zhang, Rumi Nakamura

**Methodology:** Veronika S. Grach, Andrei G. Demekhov

**Resources:** Ethan Tsai, Colin Wilkins, Owen W. Roberts

**Software:** Veronika S. Grach, Xiao-Jia Zhang

**Validation:** Jacob Bortnik

**Visualization:** Veronika S. Grach, Xiao-Jia Zhang

**Writing – original draft:** Veronika S. Grach, Anton V. Artemyev

**Writing – review & editing:** Veronika S. Grach, Andrei G. Demekhov, Xiao-Jia Zhang, Jacob Bortnik, Vassilis Angelopoulos

© 2022. American Geophysical Union.  
All Rights Reserved.

## Relativistic Electron Precipitation by EMIC Waves: Importance of Nonlinear Resonant Effects

Veronika S. Grach<sup>1</sup> , Anton V. Artemyev<sup>2</sup> , Andrei G. Demekhov<sup>1,3</sup> , Xiao-Jia Zhang<sup>2</sup> , Jacob Bortnik<sup>2</sup> , Vassilis Angelopoulos<sup>2</sup> , Rumi Nakamura<sup>4</sup> , Ethan Tsai<sup>2</sup> , Colin Wilkins<sup>2</sup> , and Owen W. Roberts<sup>4</sup> 

<sup>1</sup>Institute of Applied Physics, Russian Academy of Sciences, Nizhny Novgorod, Russia, <sup>2</sup>University of California, Los Angeles, CA, USA, <sup>3</sup>Polar Geophysical Institute, Apatity, Russia, <sup>4</sup>Space Research Institute, Austrian Academy of Science, Graz, Austria

**Abstract** Relativistic electron losses in Earth's radiation belts are usually attributed to electron resonant scattering by electromagnetic waves. One of the most important wave modes for such scattering is the electromagnetic ion cyclotron (EMIC) mode. Within the quasi-linear diffusion framework, the cyclotron resonance of relativistic electrons with EMIC waves results in very fast electron precipitation to the atmosphere. However, wave intensities often exceed the threshold for nonlinear resonant interaction, and such intense EMIC waves have been shown to transport electrons away from the loss cone due to the *force bunching* effect. In this study we investigate if this transport can block electron precipitation. We combine test particle simulations, low-altitude observations of EMIC-driven electron precipitation by the Electron Losses and Fields Investigations mission, and ground-based EMIC observations. Comparing simulations and observations, we show that, despite the low pitch-angle electrons being transported away from the loss cone, the scattering at higher pitch angles results in the loss cone filling and electron precipitation.

**Plain Language Summary** Precipitation of relativistic electrons from the Earth's radiation belts to the atmosphere has long been attributed to electron resonant scattering by electromagnetic ion cyclotron (EMIC) waves. These relativistic electron losses significantly contribute to the radiation belt dynamics, whereas precipitating electron fluxes may alter the atmosphere chemical properties. Thus, electron resonant scattering by EMIC waves has been intensively studied, in both theory and spacecraft observations. Models of two main regimes of wave-particle interactions, diffusive scattering and nonlinear resonant transport, however, predict contradicting results for electron precipitation: diffusive scattering will lead to electron losses, whereas nonlinear resonant transport may block such losses. This study combines spacecraft observations and numerical simulations to demonstrate that in reality, these two regimes work together to cause strong electron precipitation that mainly come from higher pitch angles.

## 1. Introduction

Dynamics of relativistic electron fluxes in the Earth's inner magnetosphere is largely controlled by the competition of acceleration processes (due to resonances with whistler-mode waves and/or radial transport, see, e.g., Millan & Baker, 2012; Shprits, Elkington, et al., 2008; Shprits, Subbotin, et al., 2008, and references therein) and losses, which are significantly contributed by electron resonant interaction with electromagnetic ion cyclotron (EMIC) waves (see, e.g., Blum et al., 2015; Capannolo, Li, Ma, Shen, et al., 2019; Drozdov et al., 2017; Ma et al., 2015; Miyoshi et al., 2008; Usanova et al., 2014). EMIC waves are generally much stronger than whistler-mode waves, and the resulted relativistic electron scattering can be incredibly fast (see estimates of EMIC-driven diffusion rates in Summers & Thorne, 2003; Kersten et al., 2014; Ni et al., 2015; Shprits et al., 2016). The main approach to quantify the EMIC-driven electron losses in the radiation belt models is the quasi-linear theory (e.g., Albert, 2003; Glauert & Horne, 2005; Thorne & Kennel, 1971), which operates with diffusion rates calculated under the assumption of weak wave intensity (Andronov & Trakhtengerts, 1964; Drummond & Pines, 1962; Kennel & Petschek, 1966; Vedenov et al., 1962). Spacecraft observations, however, often show EMIC wave intensities sufficiently large to exceed the threshold of quasi-linear diffusion applicability (see discussion in Wang et al., 2017; Grach et al., 2021). Therefore, an important question in modeling relativistic electron losses is how does electron scattering change for intense EMIC waves?

In contrast to diffusion by low amplitude waves, intense waves resonate with electron nonlinearity. Such nonlinear resonant interaction includes phase trapping and phase bunching, which provide direct transport of electrons in pitch-angle space (see reviews by Albert et al., 2013; Artemyev et al., 2018; Karpman, 1974; Omura et al., 1991; Shklyar & Matsumoto, 2009). For relativistic electron resonances with EMIC waves, phase bunching results in electron transport away from the loss cone (Albert & Bortnik, 2009), whereas phase trapping quickly moves electrons into the loss cone and may result in strong precipitation (Kubota & Omura, 2017; Kubota et al., 2015; Omura & Zhao, 2012, 2013). Moreover, in low pitch angles (close to the loss cone), the nonlinear wave-particle interaction is significantly modified (see, e.g., Albert et al., 2021; Artemyev, Neishtadt, et al., 2021; Kitahara & Katoh, 2019), which is particularly important for relativistic electron resonances with EMIC waves but not included in most existing models. Around the loss cone, EMIC wave interaction with electrons does not include phase trapping but is dominated by the so-called force bunching effect (Grach & Demekhov, 2020), which leads to rapid pitch-angle increases. Such direct transport away from the loss cone may block the electron precipitation (see discussion in Bortnik et al., 2022). Thus, it remains paradoxical where increased EMIC wave amplitude above the threshold of nonlinear resonant interaction may result in decreased efficiency of electron scattering into loss cone.

In this case study we focus on detailed investigation of relativistic electron scattering by intense EMIC waves. We use electron precipitation observations at low-altitude the Electron Losses and Fields Investigations (ELFIN) CubeSats (Angelopoulos et al., 2020) and conjugate EMIC wave observations at the Lovozero (LOZ) ground-based station (data acquisition system is described in Pil'gaev et al., 2021). We also use measurements from the magnetospheric multiscale (MMS) mission (Burch et al., 2016) to probe the equatorial plasma conditions important for electron resonances with EMIC waves (see Summers, 2005; Summers et al., 2007). Spacecraft and ground-based measurements are combined with test particle simulations that include realistic models of EMIC wave propagation (see Grach et al., 2021). We show that the force bunching indeed quickly moves relativistic electrons to higher pitch angles, but EMIC waves also scatter high pitch-angle electrons directly into loss cone. The competition of these two processes results in loss-cone filling and electron precipitation observed by ELFIN. The paper is structured as follows: descriptions of spacecraft and ground-based observations in Section 2, discussion of test particle simulation results in Section 3, and conclusions in Section 4.

## 2. Spacecraft Observations

Figure 1 shows the event overview with ELFIN observations of EMIC-driven electron precipitation. Energetic particle detector onboard ELFIN measures electrons in the [50, 7,000] keV energy range (16 channels,  $\Delta E/E \approx 0.4$ ) and  $\in [0, 360^\circ]$  pitch-angle range (16 sectors,  $\Delta\alpha = 22.5^\circ$ ) with a 1.5 s (half spin) resolution (Angelopoulos et al., 2020). Panel (a) shows the energy spectrum of trapped electrons (pitch angle  $\alpha \in [\alpha_{LC}, 180^\circ - \alpha_{LC}]$ , where  $\alpha_{LC}$  is the local loss-cone angle). ELFIN moved from low  $L$ -shells to higher  $L$ -shells on the dusk flank (see panel (d)), along which ELFIN traversed the plasmasphere (according to equatorial spacecraft measurements, the plasmapause is located around  $L(T89) \sim 6$ , see discussion below) and outer radiation belt. Around the plasmapause, at 13:21:05 UT, trapped electron fluxes of relativistic energies ( $>700$  keV) show a local maximum. Note that the locally trapped electrons at ELFIN map to small equatorial pitch angles, right outside the equatorial loss cone. Such transient flux increases shall be interpreted as a spatially localized enhancement of small pitch-angle electron fluxes at the equator. Panels (b and c) confirm that increases of trapped fluxes are accompanied by strong precipitation of relativistic electrons. There are two important features of this transient precipitation: First, precipitating fluxes and ratio of precipitating-to-trapped fluxes maximize at relativistic energies ( $>700$  keV) without a significant precipitation of  $<500$  keV electrons, which would indicate electron scattering by whistler-mode waves (compare the precipitation at 13:21:05 UT and precipitation likely driven by plasmaspheric hiss at 13:20:35–13:20:45 UT; also see the discussion of ELFIN observations of whistler-mode wave driven precipitation in Mourenas et al., 2021; Artemyev, Demekhov, et al., 2021; Tsai et al., 2022); Second, precipitating fluxes at relativistic energies (around  $\sim 1$  MeV) almost reach the strong diffusion limit (see the comparison of precipitating and trapped electron spectra in panel (e)). These two features strongly suggest that the observed precipitation is driven by electron scattering by EMIC waves (see similar equatorial observations of small pitch-angle flux enhancements associated with EMIC waves in Zhu et al., 2020), which resonate with relativistic electrons most effectively (Albert, 2003; Kersten et al., 2014; Ni et al., 2015; Shprits et al., 2017) and are well able to cause precipitation in the strong diffusion limit (Capannolo et al., 2022; Grach & Demekhov, 2020; Kubota & Omura, 2017; Omura & Zhao, 2013). Panels (b,e) show that in addition to the clear precipitation

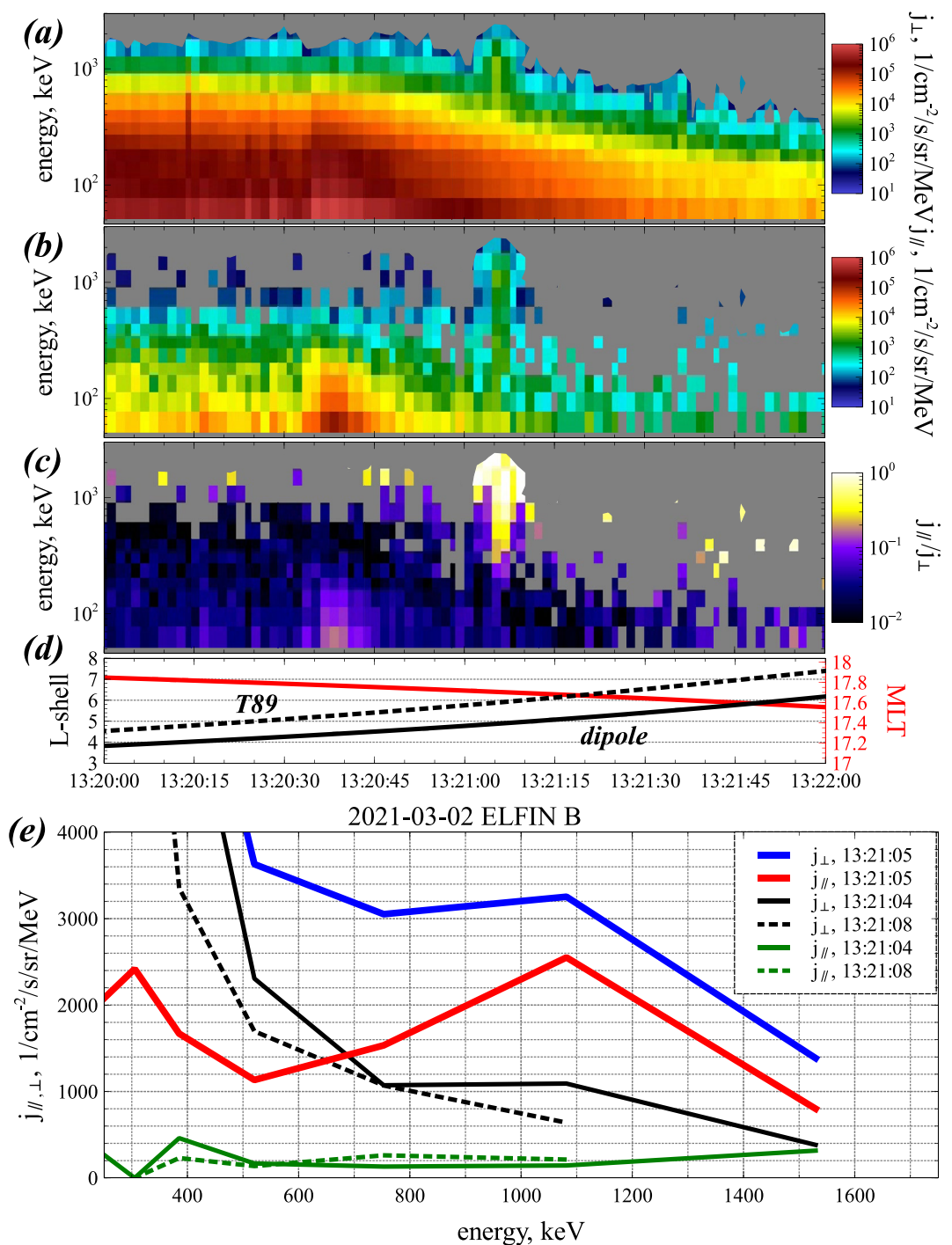


**Figure 1.** Overview of ELFIN B observations on 2 March 2021. (a) Energy spectrum of trapped electron fluxes; (b): spectrum of precipitating electron fluxes; (c) precipitating-to-trapped flux ratio; (d) ELFIN B MLT and  $L$ -shell calculated with the dipole and (Tsyganenko, 1989) magnetic field models; (e) spectra of trapped ( $\perp$ ) and precipitating ( $\parallel$ ) fluxes around the precipitation burst.

peak at  $\sim 1$  MeV, there exists moderate precipitation down to 50 keV (see discussion of low-energy electron scattering in association with EMIC waves in, e.g., Capannolo, Li, Ma, Chen, et al., 2019; Chen et al., 2016; Denton et al., 2019). Such weak electron precipitation at lower energies may be attributed to electron scattering by whistler-mode hiss waves around the plasmasphere (see discussion of hiss wave localization around the plasmasphere in, e.g., Malaspina et al., 2020).

Figure 2a shows that the ELFIN orbit with EMIC-driven electron precipitation is projected nearby the ground-based magnetometer station (LOZ), whereas the same (MLT,  $L$ -shell) region was traversed by MMS spacecraft  $\sim 1.5$  hr later. Due to the time difference between MMS and ELFIN crossings of  $L \in [6, 7]$ , field-aligned helium band EMIC waves detected by MMS (see panels (b,c)) cannot be directly associated with the precipitation at ELFIN (although the EMIC wave source region may survive for several hours, see Engebretson et al., 2015; Blum et al., 2020). Note that MMS were at middle latitudes, well below the equator, and hence cannot detect all near-equatorial EMIC waves that possibly persist after  $\sim 14:00$  UT.

We use spacecraft potential measurements (Ergun et al., 2016; Lindqvist et al., 2016; Torkar et al., 2014) and the inner magnetosphere temperature model (Boardsen et al., 2014) to estimate the cold plasma density at MMS (Andriopoulou et al., 2016, 2018). Figure 2d shows plasma density enhancements around the plasmapause, at  $L \in [8, 6]$ , with the peak density reaching  $\sim 40 \text{ cm}^{-3}$ . Such density enhancements can survive for hours (e.g., Goldstein et al., 2014), which can then guide EMIC wave propagation to the ionosphere, where after a mode conversion waves may leak to the ground with a certain spread due to propagation within ionospheric guide (Johnson & Cheng, 1999; Kim & Johnson, 2016). Although, such wave propagation and conversion may alter  $L$ -shell range of EMIC wave observations on the ground-based stations relative to the equatorial source location, ground-based observations roughly reproduce EMIC wave frequency (e.g., Blum et al., 2020; Engebretson et al., 2015, and references therein). Indeed, the LOZ station (see panel (e)) detected frequency-banded,  $\in [0.2, 1]$  Hz, waves resembling properties of EMIC emissions measured by MMS. More importantly, ground-based observations of EMIC waves are in a good conjunction with ELFIN precipitation measurements (well within expected EMIC wave source scales, see Blum et al., 2016, 2017). Therefore, we may assume that the precipitation at ELFIN is driven by helium band EMIC waves, whereas localized plasma density peaks reduce the electron resonant energies to  $\sim 1$  MeV, as shown in the precipitation energy at ELFIN. Panel (f) zooms into a ten-minute interval of ground-based measurements around the ELFIN observations. The EMIC waves measured at LOZ consist of an intense band at  $\in [0.2, 0.5]$  Hz, which does not exhibit distinguished frequency variations, and less intense wave elements ( $>0.5$  Hz) with frequency drifts, typical for rising-tone EMIC waves (e.g., Nakamura et al., 2016, 2019). We will examine electron precipitation caused by both monochromatic and rising-tone EMIC waves.

### 3. Simulation Setup and Results

To investigate the mechanism of electron precipitation observed by ELFIN, we perform a test particle simulation with observed EMIC wave characteristics. We use the dipole model of geomagnetic field  $\mathbf{B}_0$  and gyrotropic model of plasma density  $N = N_{\text{eq}} B_0 / B_{0\text{eq}}$ , where the subscript “eq” denotes equatorial values. Based on MMS measurements (see Figure 2d), we choose  $L = 6.2$ ,  $N_{\text{eq}} = 40 \text{ cm}^{-3}$ , and use the plasmaspheric ion composition  $N_{\text{H}^+} = 0.8N$ ,  $N_{\text{He}^+} = 0.2N$  from Horwitz et al. (1990). Wave packet parameters (constant wave frequency  $f = 0.95f_{\text{He}^+} = 0.48$  Hz and duration  $\tau = 120$  s) are set in agreement with ground-based (LOZ) observations; here  $f_{\text{He}^+}$  is helium gyrofrequency. We also assume a Gaussian amplitude profile with the maximum wave amplitude  $B_{\text{wm}} = 2 \text{ nT}$ . In the main text we present results for a constant wave frequency, whereas the case of wave packet with rising tone is shown in Supporting Information S1.

EMIC wave packet is generated in a small region near the equator and then propagates along the magnetic field lines. The spatial-temporal distribution of the wave field is retrieved under assumption of field-aligned wave propagation with the group velocity provided by cold plasma dispersion relation, as shown in Figure 3a (see also the distribution zoomed around the equator in panel (b)). In ray-tracing, the wave energy flux  $\mathcal{E} \propto B_w^2 V_{\text{gr}} / (8\pi)$  for each point of the packet remains constant, and the group velocity  $V_{\text{gr}}$  corresponds to the local wave dispersion relation (see details of wave model in Grach et al., 2021).

The model wave field is then used to evaluate trajectories of test electrons interacting with EMIC waves at the anomalous cyclotron resonance. We use the gyro-averaged electron equations of motion (see details in Grach & Demekhov, 2020; Grach et al., 2021):

$$\frac{dW}{dt} = -ev_{\perp}|E_w|\sin\Psi; \quad (1)$$

$$\frac{dI_{\perp}}{dt} = -\frac{2e}{mB_0}p_{\perp}(1 - n_{\parallel}\beta_{\parallel})|E_w|\sin\Psi; \quad (2)$$

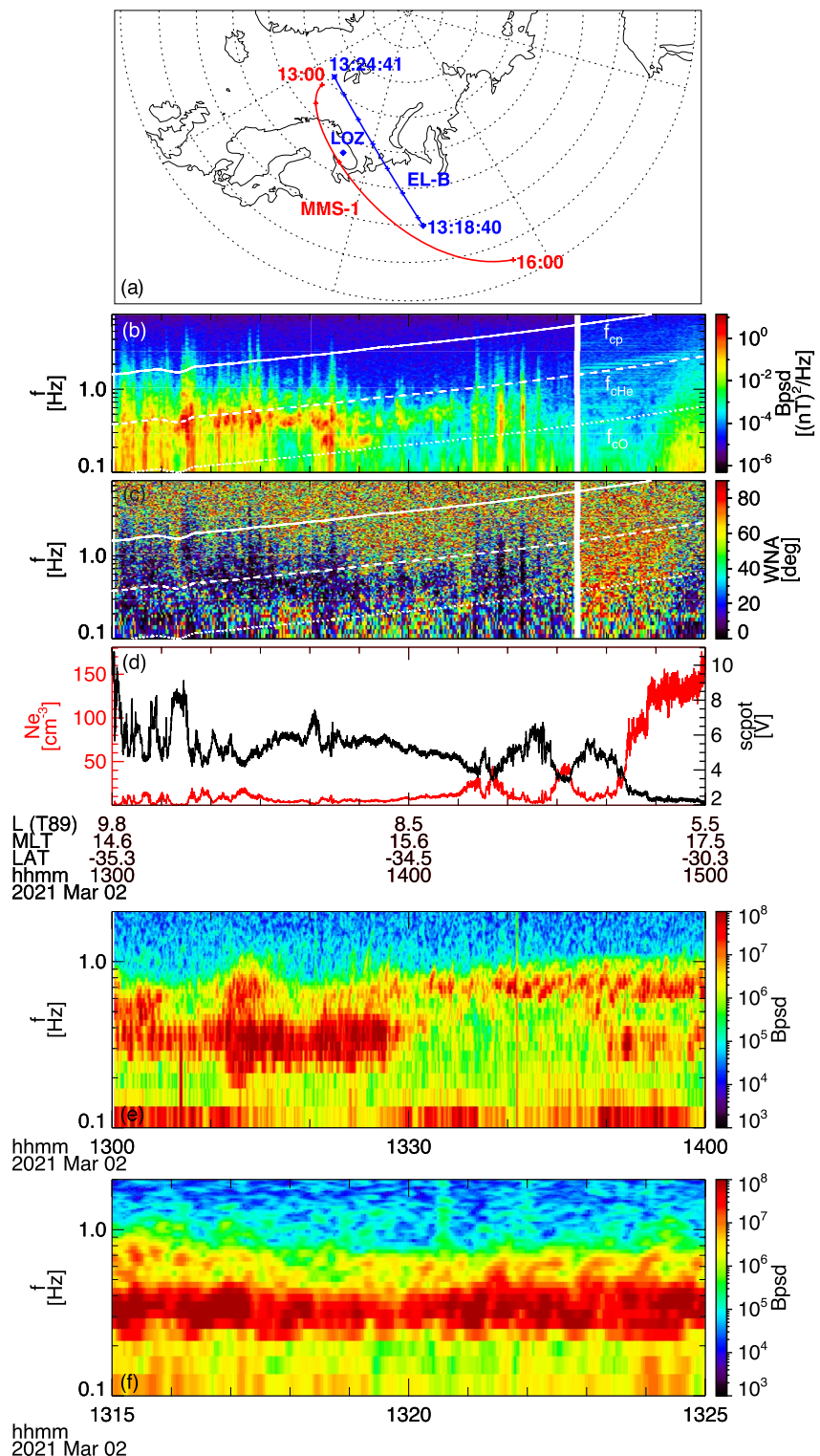


**Figure 2.** Overview of electromagnetic ion cyclotron (EMIC) wave measurements. (a) Projections of ELFIN B and magnetospheric multiscale (MMS) #1 orbits to the northern hemisphere with the ground-based LOZ station; (b): MMS magnetic field spectrum in the EMIC wave frequency range; (c) EMIC wave normal angle distributions; (d) MMS spacecraft potential and the inferred density; (e-f): spectrum of EMIC wave magnetic field measured at the LOZ station during 1 hour (e) and 10 minutes (f), separately.

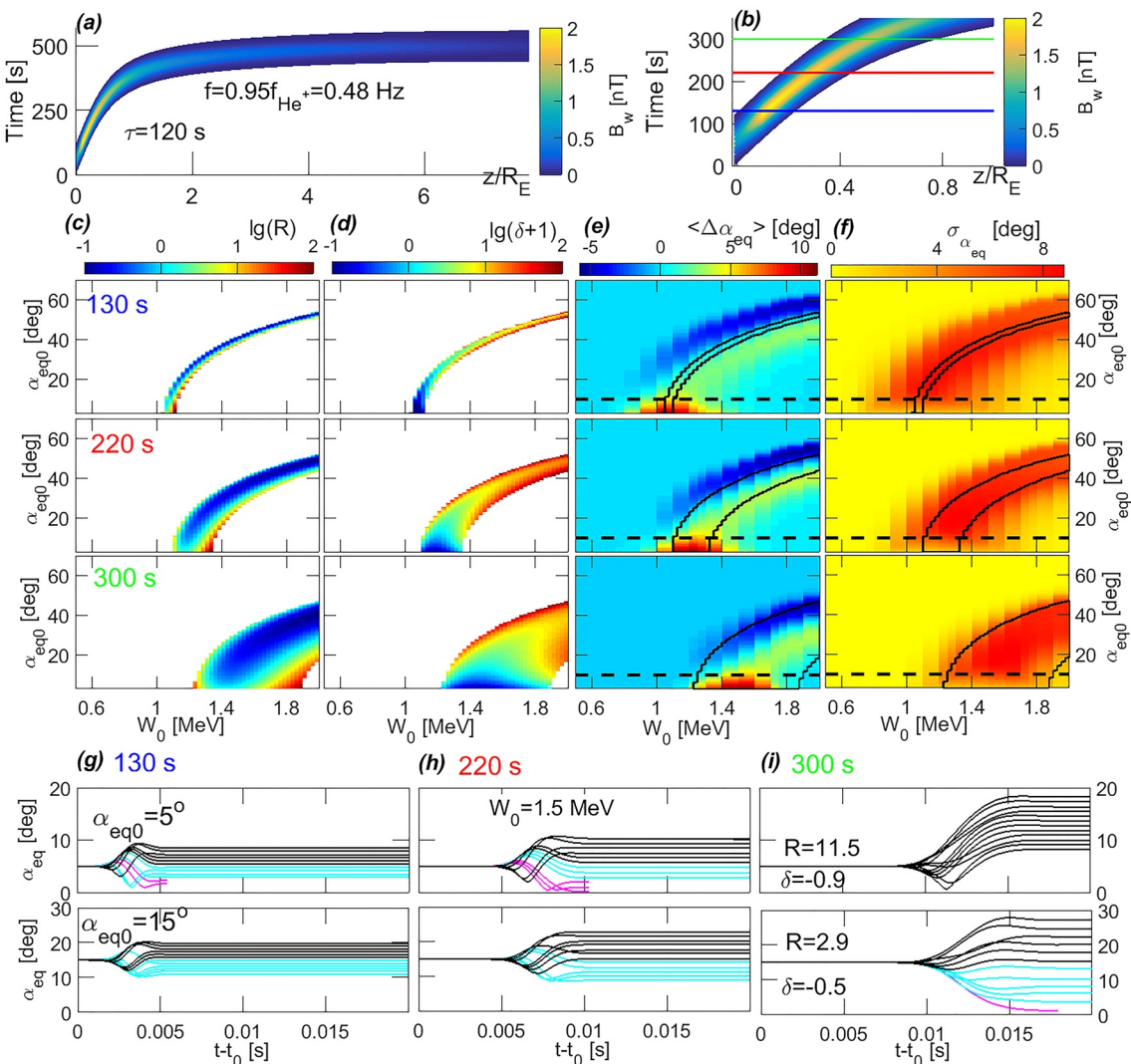


**Figure 3.** (a and b): The spatial-temporal distribution of EMIC wave field as the wave packet propagates away from its source region near the equator ( $z = 0$ ). Horizontal lines in (b) mark the start times ( $t_s$ ) of electron trajectories in three runs. (c and d): The inhomogeneity parameter  $R$  and parameter  $\delta$ . (e and f): Phase averaged change in  $\alpha_{eq}$  and rms  $\sigma_{\alpha_{eq}}$  after a single pass through the wave packet at times  $t_s$  as a function of initial energy  $W_0$  and equatorial pitch angle  $\alpha_{eq0}$ . Black traces mark unperturbed resonant domains (where the exact resonance condition with  $\Delta = 0$  is satisfied); dashed lines correspond to  $\alpha_{eq0} = 10^\circ$ . (g-i): Pitch-angle trajectories for particles with  $W_0 = 1.5$  MeV and  $\alpha_{eq0} = 5^\circ, 15^\circ$ . Black, cyan, and magenta lines correspond, respectively, to those with pitch-angle increasing, decreasing, and particles scattered into the loss cone. Values of  $R$  and  $\delta$  are shown if the unperturbed resonant point  $\Delta = 0$  exists within the wave packet.

$$\frac{d\Psi}{dt} = -\Delta - \frac{e}{p_\perp} (1 - n_\parallel \beta_\parallel) |E_w| \cos \Psi; \quad (3)$$

$$\frac{dz}{dt} = \frac{p_\parallel}{m\gamma}. \quad (4)$$

here subscripts  $\parallel$  and  $\perp$  denote projections to the parallel and transverse directions with respect to  $\mathbf{B}_0$ ;  $W = (\gamma - 1) mc^2$  and  $I_\perp = p_\perp^2 / (mB_0)$  are the electron kinetic energy and the first adiabatic invariant;  $\gamma = \sqrt{1 + [p/(mc)]^2}$  is the Lorentz factor;  $m$ ,  $p$ , and  $v$  are the electron rest mass, momentum, and velocity;  $\beta_\parallel = v_\parallel/c$ ,  $n_\parallel = kc/\omega$ ;  $\omega = 2\pi f$ ,  $k$ , and  $E_w$  are wave frequency, wave number, and slowly changing wave electric field amplitude;  $z$  is the coordinate along the geomagnetic field with  $z = 0$  corresponding to the equator;  $\Psi = \vartheta - \varphi$ ,  $\varphi$  is the gyrophase in the geomagnetic field  $\mathbf{B}_0$ ;  $\vartheta = \omega/c \int n_\parallel dz - \int \omega dt$  is the wave phase,  $\Delta = \omega - kv_\parallel + \Omega_c/\gamma$  is the mismatch from the resonance;  $\Omega_c = eB_0/mc$ , with  $e > 0$  being the elementary charge.

These equations of motion (1–4) are solved numerically by Bogacki-Shampine variant of the Runge-Kutta method. We use  $\sim 0.5 \cdot 10^6$  trajectories with 19 initial energies  $W_0 \in [0.5, 2.0]$  MeV, 135 initial equatorial pitch angles  $\alpha_{eq0} \in [3^\circ, 70^\circ]$ , and 180 initial phases uniformly distributed in  $[0, 2\pi]$ . Note that for the considered  $L$ , the loss-cone angle is  $\alpha_{eq}^{LC} \approx 2.7^\circ$ . To investigate variations of electron scattering as the wave packet evolves along magnetic field lines (see Figures 3a and 3b), we run three simulations where the electron trajectories start from the equator at times  $t_s = 130, 220$ , and 300 s, respectively.

During the interaction (linear vs. nonlinear), the particle behavior for not so small pitch angles can be approximately determined by the inhomogeneity parameter  $\mathcal{R}$  (Albert, 1993; Demekhov et al., 2006; Grach & Demekhov, 2018; Karpman et al., 1974; Omura et al., 2008). Values of  $|\mathcal{R}| = R < 1$  correspond to the possibility of particle trapping (by the wave field) and phase bunching; for the resonant interaction of relativistic electrons with EMIC waves, phase bunching leads to a pitch angle increase, trapping leads to a significant pitch angle decrease. For small pitch angles, the parameter  $\delta$  can be used to evaluate the particle behavior, as introduced in Albert et al. (2021) (or equivalently the parameter  $y_R = \delta + 1 \geq 0$  in Artemyev, Neishtadt, et al., 2021). Values of  $\delta < 0$  correspond to nonlinear resonant interactions, when the term  $\sim (E_w/p_\perp) \cos \Psi$  dominates over the  $\Delta$  term in Equation 3. Please refer to the Supporting Information S1 for the detailed definition of these two parameters. Figures 3c and 3d show maps of  $\lg R$  and  $\lg(\delta + 1) = \lg y_R$ , calculated for the unperturbed trajectories at the resonance point  $\Delta = 0$  (if it exists within the packet). As one can see, both types of nonlinear behavior are possible in the  $W_0$  and  $\alpha_{eq0}$  ranges of interest.

Electron energy remains nearly constant during the resonant interaction with EMIC waves (because the wave frequency is much smaller than electron gyrofrequency), and hence we characterize the resonant interaction by the change of equatorial pitch angles,  $\alpha_{eq}$ . We calculate the mean electron pitch angle change  $\langle \Delta \alpha_{eq} \rangle$  and spread  $\sigma_{\alpha_{eq}} = \sqrt{\langle (\Delta \alpha_{eq})^2 \rangle - \langle \Delta \alpha_{eq} \rangle^2}$  as functions of initial energy and pitch angle. Note that in this case with relatively strong wave amplitude and short packet duration, the resonant interaction zone is determined by the packet length (see Figures 3g–3i and resonant range in Figures 3c–3f), as typical for realistic EMIC wave packets (Grach & Demekhov, 2020; Grach et al., 2021).

Figures 3c and 3d show  $\langle \Delta \alpha_{eq} \rangle, \sigma_{\alpha_{eq}}$  maps for three different test particle runs (i.e., three different wave field distributions at the resonant latitudes). Electrons with small initial pitch angles show a significant  $\langle \Delta \alpha_{eq} \rangle > 0$  at the resonant energy that increases with time (with the resonant latitudes where the wave-packet intensity maximizes) from 1 to 1.5 MeV (see red regions in Figure 3e). Such a pitch-angle *reflection* from the loss cone has been found by Inan et al. (1978), Lundin & Shkliar (1977) and described for EMIC waves in Grach and Demekhov (2020) as *force bunching*. This pitch-angle increase is described by the second term on the right-hand side of Equation 3: the direct influence of Lorentz force on the particle phase is strong for small  $p_\perp$  and can exceed the inertial (or kinematic) bunching effect  $\sim \Delta$ , the first term in Equation 3. A similar behavior has been analyzed by Albert et al. (2021) and Artemyev, Neishtadt, et al. (2021) for whistler waves: the regime of resonant interactions with  $\sim (E_w/p_\perp) \cos \Psi$  term larger than  $\sim \Delta$  term in Equation 3 corresponds to  $\delta < 0$  ( $y_R < 1$ ); see the Supporting Information S1 and also discussion in Albert et al. (2022). Figures 3e and 3d show this force bunching with pitch-angle increases in test particle trajectories for the  $\delta < 0$  region (see also the statistical investigation of this effect in Bortnik et al., 2022). Comparing panels (e) and (d), we can see that in the first two cases ( $t_s = 130$  and  $t_s = 220$  s, shorter packets closer to the equator) the ranges of *force bunching* correspond to the ranges of  $\delta < 0$  (blue regions in Figure 3d) within the resonant domain, but there are also additional regions of  $\langle \Delta \alpha_{eq} \rangle > 0$  outside of it. Such an effective nonresonant interaction near the borders of the resonant domain is possible due to the large wave amplitude in this event. On the contrary, for  $t_s = 300$  s, the region of  $\langle \Delta \alpha_{eq} \rangle > 0$  is smaller than the region of  $\delta < 0$ , which results from the finite duration of the wave packet and amplitude variations within.

Figure 3c shows  $R < 1$  for a significant part of the resonant domain for not so small  $\alpha_{eq}$ , but we do not see evidence of effective nonlinear interactions in Figures 3e and 3f. There are regions of  $\langle \Delta \alpha_{eq} \rangle > 0$  (green stripes in Figure 3e) and  $\langle \Delta \alpha_{eq} \rangle < 0$  (blue stripes), but for both cases  $|\langle \Delta \alpha_{eq} \rangle|$  is not that large and  $|\langle \Delta \alpha_{eq} \rangle| < \sigma_{\alpha_{eq}}$ . Detailed analysis shows that trapping did not occur and particle trajectories of  $\alpha_{eq}(t)$  fall in to the linear regime. This is also caused by the short packet duration and realistic amplitude variations. It has been shown before, for EMIC and whistler waves, that amplitude variations can make trapping less effective (An et al., 2022; Grach & Demekhov, 2020; Grach et al., 2021; Mourenas et al., 2018; Tao et al., 2012). See the Supporting Information S1 for a comparison with a simulation using very long wave packet.

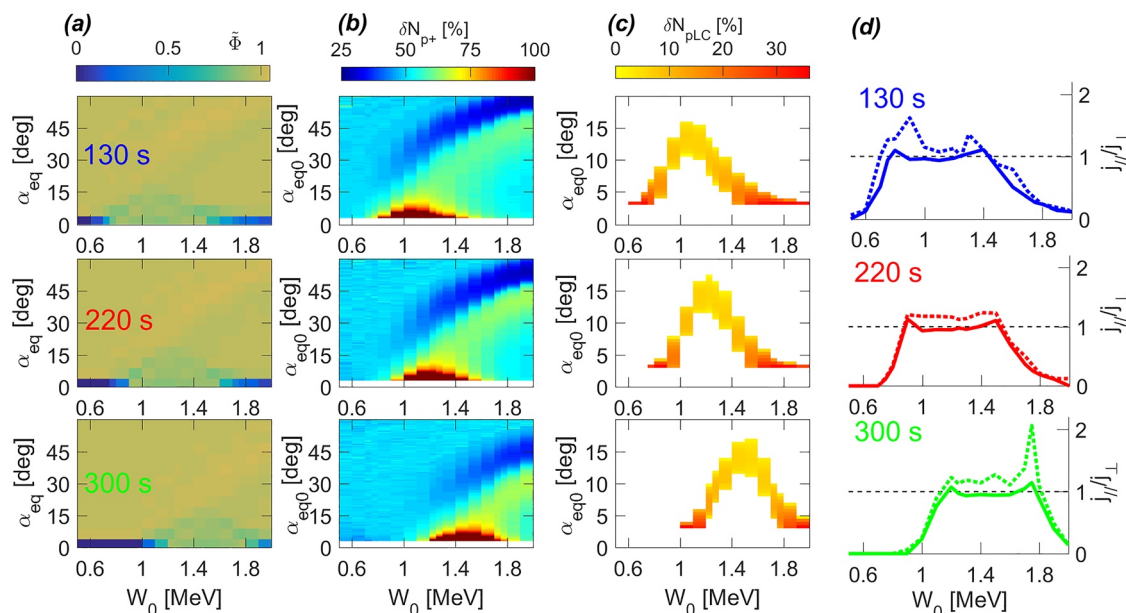


**Figure 4.** Distribution of the particle ensemble after a single pass through the wave packet. Top, middle, and bottom rows correspond to start times of 130, 220, and 300 s, respectively. (a) Pitch-angle distribution; (b and c): the fraction of particles with increased pitch angles and scattered into the loss cone, respectively; (d) The ratio between the precipitating flux and the flux of trapped particles with  $\alpha_{eq}^{LC} \leq \alpha_{eq} < \alpha_{eq}^{LC} + 5^\circ$  (solid line). Dotted lines in column (d) show the maximum ratio of the precipitating and trapped fluxes during the 5-s simulation.

For initial pitch angles  $\alpha_{eq} \approx 10^\circ\text{--}15^\circ$ , the pitch-angle drift is almost absent,  $\langle \Delta\alpha_{eq} \rangle \approx 0$ ; the pitch-angle scattering, however, is quite significant:  $\sigma_{\alpha_{eq}} > 5^\circ$  (see Figure 3f). Several test particle trajectories in Figure 3i show that such diffusive scattering (almost symmetric in the number of particles with  $\Delta\alpha_{eq} > 0$  and  $\Delta\alpha_{eq} < 0$ ) may move  $10^\circ\text{--}15^\circ$  electrons directly into the loss cone, and these electrons should precipitate to the atmosphere after a single resonant interaction.

To investigate effects of electron scattering by EMIC waves on electron dynamics, we follow the approach proposed in Grach & Demekhov 2020 and Grach et al. (2021). Assigning each test particle a specific weight, we specify an initial pitch angle distribution  $\Phi_{\alpha_{eq}}^{(0)}$  (uniform in our case) and calculate the distribution function  $\Phi_{\alpha_{eq}}$  after the wave-particle interactions. The normalized distribution  $\tilde{\Phi} = \Phi_{\alpha_{eq}} / \Phi_{\alpha_{eq}}^{(0)}$  is shown in Figure 4a. The loss cone (the smallest pitch-angle bin) is empty at the beginning, but becomes filled by electrons scattered by EMIC waves. Note that the energy range of the loss-cone filling changes with time because different energies resonate with EMIC wave-packet at different latitudes (at different times).

Figure 4b shows the percentage of particles (in each pitch-angle/energy bin) that increase their pitch angles during the simulation. This distribution mainly repeats  $\langle \Delta\alpha_{eq} \rangle$  distribution from Figure 3e. Almost all resonant electrons with small initial pitch angles move away from the loss cone ( $\delta N_{p+} \approx 100\%$ ). Resonant electrons with pitch angles above  $10^\circ$  are scattered in a diffusive way: about half electron populations increase pitch angles ( $\delta N_{p+} \approx 50\%$ ) and the other half decrease pitch angles.

Figure 4c shows distribution of percentage of electrons that are scattered directly into the loss cone after a single resonant interaction with EMIC waves. For the main energy range of resonance, a population of  $>5^\circ$  electrons ( $\sim 10\%$  of total electron population) are scattered into the loss cone. Such electrons have initial pitch angles sufficiently large to avoid the positive drift away from the loss cone (compare Figures 3e and 4c), that is, electrons can jump over the small pitch-angle range with  $\langle \Delta\alpha_{eq} \rangle > 0$  and move directly into the loss cone.

To compare simulation results with ELFIN data, we plot the ratio of the precipitating flux and flux of trapped particles with equatorial pitch angles of  $[\alpha_{eq}^{LC}, \alpha_{eq}^{LC} + 5^\circ]$ . Figure 4d shows this ratio (solid curve) as a function of energy for three time moments. The energy range [0.8, 1.8] MeV corresponds to very strong precipitation on the strong diffusion limit (with precipitating fluxes reaching the trapped flux level). Comparison of Figures 4d and 1e confirms that simulation reproduces the observed energies of strong precipitation.

We also analyzed the effects of long-term interactions, for which we run three simulations in the time interval of  $[t_s - 2.5 \text{ s}, t_s + 2.5 \text{ s}]$ , corresponding to 6–12 bounce oscillations for electrons with energies of 0.5–2 MeV. On this time scale, wave packet evolution is insignificant, so temporal dynamics is determined by the particle redistribution over pitch angles. Time averaged precipitating flux is roughly the same as in the case of the single interaction, but there are also transient bursts of precipitation deviating from the averaged level. For illustration, the maximum ratio  $j_{\parallel}/j_{\perp}$  is shown in Figure 4d as dotted lines. One can see that in some cases precipitating flux can be twice as high as the trapped flux.

Figures 3 and 4 show simulation results for a constant wave frequency, which is consistent with the predominant wave band in ground-based measurements (Figure 2). Previous investigations (e.g., Nakamura et al., 2016; Nakamura et al., 2019) have demonstrated the importance of frequency drifts in electron nonlinear resonances with EMIC waves. Therefore, we perform another simulation with rising-tone EMIC waves. As shown in Figure S2 (Supporting Information S1), the frequency drift indeed results in more effective precipitation of ultra-relativistic electrons, but significantly reduces precipitation of sub-MeV electrons. Therefore, the precipitation observed by ELFIN during this event (Figure 1) can be mostly attributed to electron resonances with the EMIC wave having a constant (or quasi-constant) frequency.

#### 4. Discussion and Conclusions

This study is focused on a detailed investigation of EMIC-driven relativistic electron precipitation as observed by ELFIN CubeSats and reproduced in numerical simulations. We aim to examine the effect of electron force bunching that moves small pitch-angle electrons away from the loss cone and may potentially block their precipitation (see Bortnik et al., 2022). Observationally driven test particle simulations show that although the force bunching indeed prevents precipitation of  $\alpha_{\text{eq}} < 10^\circ$  electrons, electrons with  $\alpha_{\text{eq}} > 10^\circ$  can still be efficiently scattered toward small pitch angles. Such a scattering may move  $\alpha_{\text{eq}} > 10^\circ$  electrons directly into the loss cone, and these electrons will be precipitated without having a chance to be transported away from the loss cone by the force bunching effect. In our event-oriented simulation, the electron precipitation is mostly diffusive, whereas the precipitation via nonlinear phase trapping by EMIC waves is effectively suppressed by the short length of EMIC wave packets. Precipitating electron measurements at low altitudes by ELFIN confirm the strong precipitation within the energy range of expectation from simulations.

Therefore, the main conclusion of this study is that the force bunching cannot completely prevent precipitation, but may change the pitch-angle range of precipitating electrons. This nonlinear effect should influence the electron pitch-angle distributions in association with EMIC waves, as measured by near-equatorial spacecraft (e.g., Bingley et al., 2019; Zhu et al., 2020), but can unlikely change the strong precipitating rate provided by EMIC waves in radiation belt models. Therefore, the force bunching must be taken into account for short-term simulations and interpretation of observations of EMIC-driven electron precipitation bursts, but may have a secondary importance for long-term simulations of radiation belt dynamics.

#### Data Availability Statement

Fluxes measured by ELFIN are available in ELFIN data archive <https://data.elfin.ucla.edu/> in CDF format. Spacecraft potential used for plasma density estimate is available on MMS data archive <https://lasp.colorado.edu/mms/sdc/public/about/browse-wrapper/>. Ground-based measurements of wave magnetic field at LOZ station are available at <http://aurora.pgia.ru:8071/index.php?p=0&s=2&x=MELZ&t=1614643200>. Data analysis was done using SPEDAS V4.1 (Angelopoulos et al., 2019). The software can be downloaded from [http://spedas.org/wiki/index.php?title=Downloads\\_and\\_Installation](http://spedas.org/wiki/index.php?title=Downloads_and_Installation).

#### References

- Albert, J. M. (1993). Cyclotron resonance in an inhomogeneous magnetic field. *Physics of Fluids B*, 5(8), 2744–2750. <https://doi.org/10.1063/1.860715>
- Albert, J. M. (2003). Evaluation of Quasi-linear diffusion coefficients for EMIC waves in a multispecies plasma. *Journal of Geophysical Research*, 108(A6), 1249. <https://doi.org/10.1029/2002JA009792>
- Albert, J. M., Artemyev, A., Li, W., Gan, L., & Ma, Q. (2022). Equations of motion near cyclotron resonance. *Frontiers in Astronomy and Space Sciences*, 9, 910224. <https://doi.org/10.3389/fspas.2022.910224>

#### Acknowledgments

The authors are grateful to NASA's CubeSat Launch Initiative for ELFIN's successful launch in the desired orbits. The authors acknowledge early support of ELFIN project by the AFOSR, under its University Nanosat Program, UNP-8 project, contract FA9453-12-D-0285, and by the California Space Grant program. The authors acknowledge critical contributions of numerous volunteer ELFIN team student members. We appreciate the access to LOZ Pe1 data (PI: Yury Fedorenko). V.S.G. acknowledges support from RSF Grant 19-72-10111 (numerical simulations in Section 3). A.V.A., X.-J.Z., and J.B. acknowledge support from the NASA Grant 80NSSC20K1270. X.-J.Z. acknowledges support from the NSF Grant 2021749. A.G.D. acknowledges support from the PGI state task funding. V.A. acknowledge support by NSF grants AGS-1242918, AGS-2019950. Analysis of the spacecraft potential data at IWF (R.N. and O. W. R.) is supported by Austrian FFG Project No. ASAP15/873685.

- Albert, J. M., Artemyev, A. V., Li, W., Gan, L., & Ma, Q. (2021). Models of resonant wave-particle interactions. *Journal of Geophysical Research: Space Physics*, 126(6), e2021JA029216. <https://doi.org/10.1029/2021JA029216>
- Albert, J. M., & Bortnik, J. (2009). Nonlinear interaction of radiation belt electrons with electromagnetic ion cyclotron waves. *Geophysical Research Letters*, 36(12), 12110. <https://doi.org/10.1029/2009GL038904>
- Albert, J. M., Tao, X., & Bortnik, J. (2013). Aspects of nonlinear wave-particle interactions. In D. Summers, I. U. Mann, D. N. Baker, & M. Schulz (Eds.), *Dynamics of the Earth's radiation belts and inner magnetosphere*. <https://doi.org/10.1029/2012GM001324>
- An, Z., Wu, Y., & Tao, X. (2022). Electron dynamics in a chorus wave field generated from particle-in-cell simulations. *Geophysical Research Letters*, 49(3), e97778. <https://doi.org/10.1029/2022GL097778>
- Andriopoulou, M., Nakamura, R., Torkar, K., Baumjohann, W., Torbert, R. B., Lindqvist, P.-A., et al. (2016). Study of the spacecraft potential under active control and plasma density estimates during the MMS commissioning phase. *Geophysical Research Letters*, 43(10), 4858–4864. <https://doi.org/10.1002/2016GL068529>
- Andriopoulou, M., Nakamura, R., Wellenzohn, S., Torkar, K., Baumjohann, W., Torbert, R. B., et al. (2018). Plasma density estimates from spacecraft potential using MMS observations in the dayside magnetosphere. *Journal of Geophysical Research: Space Physics*, 123(4), 2620–2629. <https://doi.org/10.1002/2017JA025086>
- Andronov, A. A., & Trakhtengerts, V. Y. (1964). Kinetic instability of the Earth's outer radiation belt. *Geomagnetism and Aeronomy*, 4, 233–242.
- Angelopoulos, V., Cruce, P., Drozdov, A., Grimes, E. W., Hatzigeorgiu, N., King, D. A., et al. (2019). The space physics environment data analysis system (SPEDAS). *Space Science Reviews*, 215(1), 9. <https://doi.org/10.1007/s11214-018-0576-4>
- Angelopoulos, V., Tsai, E., Bingley, L., Shaffer, C., Turner, D. L., Runov, A., et al. (2020). The ELFIN mission. *Space Science Reviews*, 216(5), 103. <https://doi.org/10.1007/s11214-020-00721-7>
- Artemyev, A. V., Demekhov, A. G., Zhang, X. J., Angelopoulos, V., Mourenas, D., Fedorenko, Y. V., et al. (2021). Role of ducting in relativistic electron loss by whistler-mode wave scattering. *Journal of Geophysical Research: Space Physics*, 126(11), e29851. <https://doi.org/10.1029/2021JA029851>
- Artemyev, A. V., Neishtadt, A. I., Albert, J. M., Gan, L., Li, W., & Ma, Q. (2021). Theoretical model of the nonlinear resonant interaction of whistler-mode waves and field-aligned electrons. *Physics of Plasmas*, 28(5), 052902. <https://doi.org/10.1063/5.0046635>
- Artemyev, A. V., Neishtadt, A. I., Vainchtein, D. L., Vasiliev, A. A., Vasko, I. Y., & Zelenyi, L. M. (2018). Trapping (capture) into resonance and scattering on resonance: Summary of results for space plasma systems. *Communications in Nonlinear Science and Numerical Simulations*, 65, 111–160. <https://doi.org/10.1016/j.cnsns.2018.05.004>
- Bingley, L., Angelopoulos, V., Sibeck, D., Zhang, X., & Halford, A. (2019). The evolution of a pitch-angle “bite-out” scattering signature caused by EMIC wave activity: A case study. *Journal of Geophysical Research: Space Physics*, 124(7), 5042–5055. <https://doi.org/10.1029/2018JA026292>
- Blum, L. W., Agapitov, O., Bonnell, J. W., Kletzing, C., & Wygant, J. (2016). EMIC wave spatial and coherence scales as determined from multi-point Van Allen probe measurements. *Geophysical Research Letters*, 43(10), 4799–4807. <https://doi.org/10.1002/2016GL068799>
- Blum, L. W., Bonnell, J. W., Agapitov, O., Paulson, K., & Kletzing, C. (2017). EMIC wave scale size in the inner magnetosphere: Observations from the dual Van Allen Probes. *Geophysical Research Letters*, 44(3), 1227–1233. <https://doi.org/10.1002/2016GL072316>
- Blum, L. W., Halford, A., Millan, R., Bonnell, J. W., Goldstein, J., Usanova, M., et al. (2015). Observations of coincident EMIC wave activity and duskside energetic electron precipitation on 18–19 January 2013. *Geophysical Research Letters*, 42(14), 5727–5735. <https://doi.org/10.1002/2015GL065245>
- Blum, L. W., Remya, B., Denton, M. H., & Schiller, Q. (2020). Persistent EMIC wave activity across the nightside inner magnetosphere. *Geophysical Research Letters*, 47(6), e87009. <https://doi.org/10.1029/2020GL087009>
- Boardsen, S. A., Adrian, M. L., Pfaff, R., & Menietti, J. D. (2014). Inner magnetospheric electron temperature and spacecraft potential estimated from concurrent Polar upper hybrid frequency and relative potential measurements. *Journal of Geophysical Research: Space Physics*, 119(10), 8046–8062. <https://doi.org/10.1002/2014JA019852>
- Bortnik, J., Albert, J., Artemyev, A., Li, W., Jun, C.-W., Grach, V., & Demekhov, A. (2022). Amplitude dependence of nonlinear precipitation blocking of relativistic electrons by large amplitude EMIC waves. *Geophysical Research Letters*, 49(12). <https://doi.org/10.1029/2022GL098365>
- Burch, J. L., Moore, T. E., Torbert, R. B., & Giles, B. L. (2016). Magnetospheric multiscale overview and science objectives. *Space Science Reviews*, 199(1–4), 5–21. <https://doi.org/10.1007/s11214-015-0164-9>
- Capannolo, L., Li, W., Ma, Q., Chen, L., Shen, X. C., Spence, H. E., et al. (2019). Direct observation of sub-relativistic electron precipitation potentially driven by EMIC waves. *Geophysical Research Letters*, 46(22), 12711–12721. <https://doi.org/10.1029/2019GL084202>
- Capannolo, L., Li, W., Ma, Q., Shen, X. C., Zhang, X. J., Redmon, R. J., et al. (2019). Energetic electron precipitation: Multievent analysis of its spatial extent during emic wave activity. *Journal of Geophysical Research: Space Physics*, 124(4), 2466–2483. <https://doi.org/10.1029/2018JA026291>
- Capannolo, L., Li, W., Millan, R., Smith, D., Sivadas, N., Sample, J., & Shekhar, S. (2022). Relativistic electron precipitation near midnight: Drivers, distribution, and properties. *Journal of Geophysical Research: Space Physics*, 127(1), e2021JA030111. <https://doi.org/10.1029/2021JA030111>
- Chen, L., Thorne, R. M., Bortnik, J., & Zhang, X.-J. (2016). Nonresonant interactions of electromagnetic ion cyclotron waves with relativistic electrons. *Journal of Geophysical Research*, 121(10), 9913–9925. <https://doi.org/10.1002/2016JA022813>
- Demekhov, A. G., Trakhtengerts, V. Y., Rycroft, M. J., & Nunn, D. (2006). Electron acceleration in the magnetosphere by whistler-mode waves of varying frequency. *Geomagnetism and Aeronomy*, 46(6), 711–716. <https://doi.org/10.1134/S0016793206060053>
- Denton, R. E., Ofman, L., Shprits, Y. Y., Bortnik, J., Millan, R. M., Rodger, C. J., et al. (2019). Pitch angle scattering of sub-MeV relativistic electrons by electromagnetic ion cyclotron waves. *Journal of Geophysical Research: Space Physics*, 124(7), 5610–5626. <https://doi.org/10.1029/2018JA026384>
- Drozdov, A. Y., Shprits, Y. Y., Usanova, M. E., Aseev, N. A., Kellerman, A. C., & Zhu, H. (2017). EMIC wave parameterization in the long-term VERB code simulation. *Journal of Geophysical Research*, 122(8), 8488–8501. <https://doi.org/10.1002/2017JA024389>
- Drummond, W. E., & Pines, D. (1962). Nonlinear stability of plasma oscillations. *Nuclear Fusion Suppl*, 3, 1049–1058.
- Engelbreton, M. J., Posch, J. L., Wygant, J. R., Kletzing, C. A., Lessard, M. R., Huang, C.-L., et al. (2015). Van Allen probes, NOAA, GOES, and ground observations of an intense EMIC wave event extending over 12 h in magnetic local time. *Journal of Geophysical Research*, 120(7), 5465–5488. <https://doi.org/10.1002/2015JA021227>
- Ergun, R. E., Tucker, S., Westfall, J., Goodrich, K. A., Malaspina, D. M., Summers, D., et al. (2016). The axial double probe and fields signal processing for the MMS mission. *Space Science Reviews*, 199(1–4), 167–188. <https://doi.org/10.1007/s11214-014-0115-x>
- Glauert, S. A., & Horne, R. B. (2005). Calculation of pitch angle and energy diffusion coefficients with the PADIE code. *Journal of Geophysical Research*, 110(A9), 4206. <https://doi.org/10.1029/2004JA010851>
- Goldstein, J., de Pascuale, S., Kletzing, C., Kurth, W., Genestreti, K. J., Skoug, R. M., et al. (2014). Simulation of Van Allen probes plasmapause encounters. *Journal of Geophysical Research*, 119(9), 7464–7484. <https://doi.org/10.1002/2014JA020252>

- Grach, V. S., & Demekhov, A. G. (2018). Resonance interaction of relativistic electrons with ion-cyclotron waves. I. Specific features of the nonlinear interaction regimes. *Radiophysics and Quantum Electronics*, 60(12), 942–959. <https://doi.org/10.1007/s11141-018-9860-0>
- Grach, V. S., & Demekhov, A. G. (2020). Precipitation of relativistic electrons under resonant interaction with electromagnetic ion cyclotron wave packets. *Journal of Geophysical Research: Space Physics*, 125(2), e27358. <https://doi.org/10.1029/2019JA027358>
- Grach, V. S., Demekhov, A. G., & Larchenko, A. V. (2021). Resonant interaction of relativistic electrons with realistic electromagnetic ion-cyclotron wave packets. *Earth Planets and Space*, 73(1), 129. <https://doi.org/10.1186/s40623-021-01453-w>
- Horwitz, J. L., Comfort, R. H., Richards, P. G., Chandler, M. O., Chappell, C. R., Anderson, P., et al. (1990). Plasmasphere-ionosphere coupling 2. Ion composition measurements at plasmaspheric and ionospheric altitudes and comparison with modeling results. *Journal of Geophysical Research*, 95(A6), 7949–7959. <https://doi.org/10.1029/JA095iA06p07949>
- Inan, U. S., Bell, T. F., & Helliwell, R. A. (1978). Nonlinear pitch angle scattering of energetic electrons by coherent VLF waves in the magnetosphere. *Journal of Geophysical Research*, 83(A7), 3235–3254. <https://doi.org/10.1029/JA083iA07p03235>
- Johnson, J. R., & Cheng, C. Z. (1999). Can ion cyclotron waves propagate to the ground? *Geophysical Research Letters*, 26(6), 671–674. <https://doi.org/10.1029/1999GL900074>
- Karpman, V. I. (1974). Nonlinear effects in the ELF waves propagating along the magnetic field in the magnetosphere. *Space Science Reviews*, 16(3), 361–388. <https://doi.org/10.1007/BF00171564>
- Karpman, V. I., Istomin, J. N., & Shklyar, D. R. (1974). Nonlinear theory of a quasi-monochromatic whistler mode packet in inhomogeneous plasma. *Plasma Physics*, 16(8), 685–703. <https://doi.org/10.1088/0032-1028/16/8/001>
- Kennel, C. F., & Petschek, H. E. (1966). Limit on stably trapped particle fluxes. *Journal of Geophysical Research*, 71, 1–28. <https://doi.org/10.1029/jz071i001p0001>
- Kersten, T., Horne, R. B., Glauert, S. A., Meredith, N. P., Fraser, B. J., & Grew, R. S. (2014). Electron losses from the radiation belts caused by EMIC waves. *Journal of Geophysical Research*, 119(11), 8820–8837. <https://doi.org/10.1002/2014JA020366>
- Kim, E.-H., & Johnson, J. R. (2016). Full-wave modeling of EMIC waves near the He+ gyrofrequency. *Geophysical Research Letters*, 43(1), 13–21. <https://doi.org/10.1002/2015GL066978>
- Kitahara, M., & Katoh, Y. (2019). Anomalous trapping of low pitch angle electrons by coherent whistler mode waves. *Journal of Geophysical Research*, 124(7), 5568–5583. <https://doi.org/10.1029/2019JA026493>
- Kubota, Y., & Omura, Y. (2017). Rapid precipitation of radiation belt electrons induced by EMIC rising tone emissions localized in longitude inside and outside the plasmapause. *Journal of Geophysical Research: Space Physics*, 122(1), 293–309. <https://doi.org/10.1002/2016JA023267>
- Kubota, Y., Omura, Y., & Summers, D. (2015). Relativistic electron precipitation induced by EMIC-triggered emissions in a dipole magnetosphere. *Journal of Geophysical Research: Space Physics*, 120(6), 4384–4399. <https://doi.org/10.1002/2015JA021017>
- Lindqvist, P.-A., Olsson, G., Torbert, R. B., King, B., Granoff, M., Rau, D., et al. (2016). The spin-plane double probe electric field instrument for MMS. *Space Science Reviews*, 199(1–4), 137–165. <https://doi.org/10.1007/s11214-014-0116-9>
- Lundin, B. V., & Shkliar, D. R. (1977). Interaction of electrons with low transverse velocities with VLF waves in an inhomogeneous plasma. *Geomagnetism and Aeronomy*, 17, 246–251.
- Ma, Q., Li, W., Thorne, R. M., Ni, B., Kletzing, C. A., Kurth, W. S., et al. (2015). Modeling inward diffusion and slow decay of energetic electrons in the Earth's outer radiation belt. *Geophysical Research Letters*, 42(4), 987–995. <https://doi.org/10.1002/2014GL062977>
- Malaspina, D. M., Zhu, H., & Drozdov, A. Y. (2020). A wave model and diffusion coefficients for plasmaspheric hiss parameterized by plasma-pause location. *Journal of Geophysical Research: Space Physics*, 125(2), e27415. <https://doi.org/10.1029/2019JA027415>
- Millan, R. M., & Baker, D. N. (2012). Acceleration of particles to high energies in Earth's radiation belts. *Space Science Reviews*, 173(1–4), 103–131. <https://doi.org/10.1007/s11214-012-9941-x>
- Miyoshi, Y., Sakaguchi, K., Shiokawa, K., Evans, D., Albert, J., Connors, M., & Jordanova, V. (2008). Precipitation of radiation belt electrons by EMIC waves, observed from ground and space. *Geophysical Research Letters*, 35(23), L23101. <https://doi.org/10.1029/2008GL035727>
- Mourenas, D., Artemyev, A. V., Zhang, X. J., Angelopoulos, V., Tsai, E., & Wilkins, C. (2021). Electron lifetimes and diffusion rates inferred from ELFIN measurements at low altitude: First results. *Journal of Geophysical Research: Space Physics*, 126(11), e29757. <https://doi.org/10.1029/2021JA029757>
- Mourenas, D., Zhang, X.-J., Artemyev, A. V., Angelopoulos, V., Thorne, R. M., Bortnik, J., et al. (2018). Electron nonlinear resonant interaction with short and intense parallel chorus wave packets. *Journal of Geophysical Research*, 123(6), 4979–4999. <https://doi.org/10.1029/2018JA025417>
- Nakamura, S., Omura, Y., & Angelopoulos, V. (2016). A statistical study of EMIC rising and falling tone emissions observed by THEMIS. *Journal of Geophysical Research: Space Physics*, 121(9), 8374–8391. <https://doi.org/10.1002/2016JA022353>
- Nakamura, S., Omura, Y., Kletzing, C., & Baker, D. N. (2019). Rapid precipitation of relativistic electron by EMIC rising-tone emissions observed by the Van Allen probes. *Journal of Geophysical Research: Space Physics*, 124(8), 6701–6714. <https://doi.org/10.1029/2019JA026772>
- Ni, B., Cao, X., Zou, Z., Zhou, C., Gu, X., Bortnik, J., et al. (2015). Resonant scattering of outer zone relativistic electrons by multiband EMIC waves and resultant electron loss time scales. *Journal of Geophysical Research*, 120(9), 7357–7373. <https://doi.org/10.1002/2015JA021466>
- Omura, Y., Katoh, Y., & Summers, D. (2008). Theory and simulation of the generation of whistler-mode chorus. *Journal of Geophysical Research*, 113(A4), 4223. <https://doi.org/10.1029/2007JA012622>
- Omura, Y., Matsumoto, H., Nunn, D., & Rycroft, M. J. (1991). A review of observational, theoretical and numerical studies of VLF triggered emissions. *Journal of Atmospheric and Terrestrial Physics*, 53(5), 351–368. [https://doi.org/10.1016/0021-9169\(91\)90031-2](https://doi.org/10.1016/0021-9169(91)90031-2)
- Omura, Y., & Zhao, Q. (2012). Nonlinear pitch angle scattering of relativistic electrons by EMIC waves in the inner magnetosphere. *Journal of Geophysical Research*, 117(A16), 8227. <https://doi.org/10.1029/2012JA017943>
- Omura, Y., & Zhao, Q. (2013). Relativistic electron microbursts due to nonlinear pitch angle scattering by EMIC triggered emissions. *Journal of Geophysical Research*, 118(8), 5008–5020. <https://doi.org/10.1002/jgra.50477>
- Pil'gaev, S. V., Larchenko, A. V., Fedorenko, Y. V., Filatov, M. V., & Nikitenko, A. S. (2021). A three-component very-low-frequency signal receiver with precision data synchronization with universal time. *Instruments and Experimental Techniques*, 64(5), 744–753. <https://doi.org/10.1134/s0020441221040229>
- Shklyar, D. R., & Matsumoto, H. (2009). Oblique whistler-mode waves in the inhomogeneous magnetospheric plasma: Resonant interactions with energetic charged particles. *Surveys in Geophysics*, 30(2), 55–104. <https://doi.org/10.1007/s10712-009-9061-7>
- Shprits, Y. Y., Drozdov, A. Y., Spasojevic, M., Kellerman, A. C., Usanova, M. E., Engebretson, M. J., et al. (2016). Wave-induced loss of ultra-relativistic electrons in the Van Allen radiation belts. *Nature Communications*, 7(1), 12883. <https://doi.org/10.1038/ncomms12883>
- Shprits, Y. Y., Elkington, S. R., Meredith, N. P., & Subbotin, D. A. (2008). Review of modeling of losses and sources of relativistic electrons in the outer radiation belt I: Radial transport. *Journal of Atmospheric and Solar-Terrestrial Physics*, 70(14), 1679–1693. <https://doi.org/10.1016/j.jastp.2008.06.008>
- Shprits, Y. Y., Kellerman, A., Aseev, N., Drozdov, A. Y., & Michaelis, I. (2017). Multi-MeV electron loss in the heart of the radiation belts. *Geophysical Research Letters*, 44(3), 1204–1209. <https://doi.org/10.1002/2016GL072258>

- Shprits, Y. Y., Subbotin, D. A., Meredith, N. P., & Elkington, S. R. (2008). Review of modeling of losses and sources of relativistic electrons in the outer radiation belt II: Local acceleration and loss. *Journal of Atmospheric and Solar-Terrestrial Physics*, 70(14), 1694–1713. <https://doi.org/10.1016/j.jastp.2008.06.014>
- Summers, D. (2005). Quasi-linear diffusion coefficients for field-aligned electromagnetic waves with applications to the magnetosphere. *Journal of Geophysical Research*, 110(A9), 8213. <https://doi.org/10.1029/2005JA011159>
- Summers, D., Ni, B., & Meredith, N. P. (2007). Timescales for radiation belt electron acceleration and loss due to resonant wave-particle interactions: 2. Evaluation for VLF chorus, ELF hiss, and electromagnetic ion cyclotron waves. *Journal of Geophysical Research*, 112(A11), 4207. <https://doi.org/10.1029/2006JA011993>
- Summers, D., & Thorne, R. M. (2003). Relativistic electron pitch-angle scattering by electromagnetic ion cyclotron waves during geomagnetic storms. *Journal of Geophysical Research*, 108(A4), 1143. <https://doi.org/10.1029/2002JA009489>
- Tao, X., Bortnik, J., Thorne, R. M., Albert, J. M., & Li, W. (2012). Effects of amplitude modulation on nonlinear interactions between electrons and chorus waves. *Geophysical Research Letters*, 39(6), L06102. <https://doi.org/10.1029/2012GL051202>
- Thorne, R. M., & Kennel, C. F. (1971). Relativistic electron precipitation during magnetic storm main phase. *Journal of Geophysical Research*, 76(19), 4446–4453. <https://doi.org/10.1029/JA076i19p04446>
- Torkar, K., Nakamura, R., Tajmar, M., Scharlemann, C., Jeszenszky, H., Laky, G., et al. (2014). Active spacecraft potential control investigation. *Space Science Reviews*, 199(1–4), 515–544. <https://doi.org/10.1007/s11214-014-0049-3>
- Tsai, E., Artemyev, A., Zhang, X.-J., & Angelopoulos, V. (2022). Relativistic electron precipitation driven by nonlinear resonance with whistler-mode waves. *Journal of Geophysical Research: Space Physics*, 127(5), e2022JA030338. <https://doi.org/10.1029/2022JA030338>
- Tsyganenko, N. A. (1989). A magnetospheric magnetic field model with a warped tail current sheet. *Planetary and Space Science*, 37(1), 5–20. [https://doi.org/10.1016/0032-0633\(89\)90066-4](https://doi.org/10.1016/0032-0633(89)90066-4)
- Usanova, M. E., Drozdov, A., Orlova, K., Mann, I. R., Shprits, Y., Robertson, M. T., et al. (2014). Effect of EMIC waves on relativistic and ultra-relativistic electron populations: Ground-based and Van Allen Probes observations. *Geophysical Research Letters*, 41(5), 1375–1381. <https://doi.org/10.1002/2013GL059024>
- Vedenov, A. A., Velikhov, E., & Sagdeev, R. (1962). Quasilinear theory of plasma oscillations. *Nuclear Fusion Suppl*(2), 465–475.
- Wang, G., Su, Z., Zheng, H., Wang, Y., Zhang, M., & Wang, S. (2017). Nonlinear fundamental and harmonic cyclotron resonant scattering of radiation belt ultrarelativistic electrons by oblique monochromatic emic waves. *Journal of Geophysical Research*, 122(2), 1928–1945. <https://doi.org/10.1002/2016JA023451>
- Zhu, H., Chen, L., Claudepierre, S. G., & Zheng, L. (2020). Direct evidence of the pitch angle scattering of relativistic electrons induced by EMIC waves. *Geophysical Research Letters*, 47(4), e85637. <https://doi.org/10.1029/2019GL085637>